

Research Article

A Simple Solution and Dilatancy Characterization for a Circular Tunnel Excavated in the Nonlinear Strain-Softening and Nonlinear Dilatancy Rock Mass

Xiuling Wang ^{1,2}

¹China Railway First Survey and Design Institute Group Co., Ltd., Xi'an 710043, China

²Shaanxi Railway and Underground Traffic Engineering Key Laboratory (FSDI), Xi'an 710043, China

Correspondence should be addressed to Xiuling Wang; wangxiuling@chd.edu.cn

Received 25 December 2022; Revised 30 March 2023; Accepted 26 May 2023; Published 2 June 2023

Academic Editor: Zhipeng Zhao

Copyright © 2023 Xiuling Wang. This is an open access article distributed under the Creative Commons Attribution License, which permits unrestricted use, distribution, and reproduction in any medium, provided the original work is properly cited.

Tunnel opening or excavation in the strain-softening rock masses primarily leads to initial stress release and rock deformation. The increasing plastic shear strain induces a nonlinear variation of dilatancy in rock masses. Therefore, tunnel stability is strongly dependent on the stress state and the strain-softening and dilatancy behaviors of rock masses. In view of this, this paper proposes an elastoplastic finite difference solution based on the triple-shear element (TS) unified strength criterion (USC) and the nonassociative flow law; thereafter, some typical examples are referred to verify its validity. This solution allows for the description of the intermediate principal stress effect, the nonlinear strain-softening and dilatancy behaviors of the rock mass. Parametric analysis finally determines the influence characteristics of the intermediate principal stress effect (b), the critical softening parameter (η^*), softening factor (δ), and support force (p_i) on the dilation angle (ψ) of the rock mass in the plastic zone. The findings confirm that the intermediate principal stress mainly affects peak values of ψ , which increases as b grows. The rate of change of ψ mainly depends on η^* , which tends to be slower with increasing η^* . The variation pattern of ψ in the residual zone under different δ is generally consistent, while the variability of ψ in the softening zone is significant. For a given intermediate principal stress state and strain-softening behavior of the rock mass, the values and the developed form of ψ in the plastic zone is independent of p_i .

1. Introduction

The elastoplastic analysis of underground excavation or opening under axisymmetric conditions has been a classical mechanical issue [1–3], and a considerable number of studies have been performed on rock stress and strain determination [4, 5]. These achievements are utilized to develop ground reaction curves (GRCs) for tunnels with different shapes, excavated in rock masses of different qualities with varying stress states [6, 7], which are further used for tunnel design and response analysis [8, 9].

The stability or elastic-plastic state of rock masses are primarily described by various strength criteria [10], while the majority of the elastoplastic analysis was performed on the circular tunnels excavated in the rock materials compatible with the two-dimensional Mohr–Coulomb (M-C) or

Hoek–Brown (H-B) criterion [11, 12]. However, numerous findings from in situ stress measurements demonstrate that deep openings are usually dominated by the pronounced three-dimensional unequal stress conditions [13–15]. Also, most studies are conducted on the basis of the consideration of the maximum and minimum principal stresses, where the effect of the intermediate principal stress effect on mechanical properties of the rock mass has been neglected. This is detrimental to the design of the tunnel support system [16, 17].

Additionally, other achievements obtained from the experiments [18], numerical simulations [19], and theoretical analyses [20] emphasize the role of the intermediate principal stress in the strength potential and self-stabilizing effect of the rock masses. For example, Kabwe [21] achieved the consideration of intermediate principal stress effect in

the proposed numerical solution by the inclusion of the stress Lode parameter in the circumscribed Drucker–Prager (D-P) yield criterion and further suggested that yield criteria accounting for the intermediate principal stress effect should be employed in analytical solutions to gain an accurate ground reaction estimation. Some other researchers also noted that the rock mass strength depends entirely on the intermediate principal stress, which acts as the confining stress [18, 22]. These also reflect the problem of conservativeness of tunnel design based on the two-dimensional theory [23]. Therefore, a strength criterion with a nonlinear strength envelope is indispensable for accurate descriptions of rock mechanical behaviors.

The three-dimensional USC proposed by Yu [24] for geotechnical materials can address the limitations that traditional yield criteria fail to consider the intermediate principal stress effect. This criterion was derived from the twin-shear element unified strength theory and takes into account the effects of all the three principal stresses [25]. Thereafter, the criterion is adopted for elastoplastic analysis of a tunnel excavated in elastic-perfectly-plastic (EPP) rock mass, in which the intermediate principal stress was assumed to act along the tunnel axis [26]. Zhang et al. [27] proposed solutions for radial displacement and support force of a tunnel built in the USC rock mass. Subsequently, the USC yield criterion has been successfully employed in studies, e.g., [28, 29]. As for a yield criterion considering all the three principal stresses, the USC has proved to be an alternative. In the follow-up studies, the double slip angle phenomenon occurs in twin-shear element USC for some specific stress states [30]. To overcome this unfavorable situation, Hu and Yu [30] further proposed the triple-shear element USC (TS-USC), which takes into account the effect of all the principal shear stresses on the yield failure. It provides an effective solution for mechanical response analysis of geotechnical materials [31, 32].

In rock mechanics and geomechanics, precise descriptions of rock mass behaviors remain the most challenging task, especially for the mechanical properties in the postfailure stage, as it significantly affects the stability of the rock mass [33]. Although there are lots of analytical solutions or approaches to characterize the elastic-plastic response of the rock masses, most of them are based on the EPP [17, 34] or elastic-brittle (EB) [35, 36] rock masses. Nevertheless, a large number of underground excavation or opening involves the soft rock strata, where these average quality rock masses are characterized by the strain-softening [37, 38] and dilatancy behaviors [39, 40]. To analyze the strain-softening behaviors of the rock masses in a tunnel, Lee and Pietruszczak [41] and Park et al. [42] proposed methods to divide the potential plastic zone into concentric rings. Based on these methods, many research studies have been performed on the deformation and failure of the rock masses [43–45]; however, the dilation angle in these solutions was simplified as a constant or linear parameter. Dilatancy is closely associated with the process of deformation and failure of the rock masses [46, 47], and thus, the dilation angle should not be oversimplified in the elastoplastic analysis.

Yi et al. [48] also stated that strain-softening and dilatancy behaviors in rock masses bring a significant synergistic effect, and considerable errors would be induced if neglecting the strain softening and dilatancy during a deep tunnel analysis. Therefore, it is more appropriate to investigate rock displacement laws and tunnel stability with considering the strain-softening and dilatancy behaviors of rock masses.

As a result of this review, it turns out that the intermediate principal stress effect, strain softening, and dilatancy all exert notable influence on the tunnel stability and should be evaluated for accurately computing the stresses and displacements around the excavated tunnels. This study mainly aims to develop a simple numerical solution for displacements and stresses determination of the tunnels surrounded by the rock mass exhibiting the strain-softening and dilatancy behaviors. The present paper is organized as follows. The second section states the derivation framework. In this section, the TS-USC, the nonlinear strain-softening model, and the nonlinear dilatancy model are applied to describe the intermediate principal stress effect as well as the postfailure behaviors of the rock masses. In the third section, with reference to the finite difference method proposed by Lee and Pietruszczak [41], the numerical solutions for the stresses and displacements are derived for the strain-softening and dilatancy rock masses. In the fourth section, some published rigorous algorithms, as well as the illustrative example, are referred and compared to confirm the validity of the proposed solution. In the fifth section, a parametric analysis is conducted to evaluate the influence of some typical parameters on the dilatancy response of rock masses, and some discussions and suggestions are then presented. The study has been technically concluded in the last section.

2. Statement of the Problem

2.1. Problem Definition. The problem is defined in Figure 1, where a circular tunnel with a radius of R_0 is subjected to hydrostatic stress field σ_0 . The support structure provides a uniformly distributed radial support force p_i at the excavation surface, and the radii of plastic and residual zones in the rock mass are R_p and R_s , respectively. The tangential and radial stresses at the elastic-plastic interface of the rock mass are $\sigma_{\theta p}$ and σ_{rp} , respectively. When p_i is less than p_i^* (p_i^* is the support force at the interface of the softening and residual zone), the softening zone continues to develop and then yields the residual zone. The rock strength in the softening zone gradually decreases to the residual value. The tangential and radial stresses at the softening and residual zone interface are $\sigma_{\theta s}$ and σ_{rs} , respectively.

2.2. Triple-Shear Element Unified Strength Criterion. The TS-USC comprehensively captures the basic strength properties of rocks, such as the tensile and compressive inequalities and the intermediate principal stress effect. The

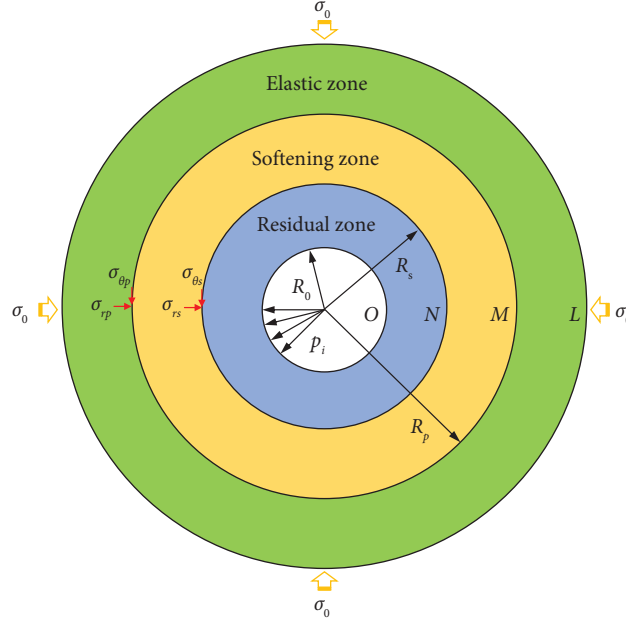


FIGURE 1: Schematic diagram for a circular opening used for problem definition.

double slip angle problem observed in twin-shear element USC for some specific stress states is also overcome. It is expressed as follows [30]:

$$(\sigma_1 - \alpha\sigma_3)(\sigma_1 - \sigma_3) + b(\sigma_1 - \alpha\sigma_2)(\sigma_1 - \sigma_2) + b(\sigma_2 - \alpha\sigma_3)(\sigma_2 - \sigma_3) = (1 + b)(\sigma_1 - \sigma_3)\sigma_t, \quad (1)$$

where σ_1 , σ_2 , and σ_3 are the maximum, intermediate, and minimum principal stresses; $\sigma_t = (2c \cos \varphi)/(1 + \sin \varphi)$, $\alpha = (1 - \sin \varphi)/(1 + \sin \varphi)$; c and φ are the cohesion and the angle of internal friction; and b is the intermediate principal stress influence parameter. The values of b that satisfies the externally convex type of plane π -limit line is as follows [24]:

$$0 \leq b \leq b_{\max} = \frac{\alpha}{2 + \alpha}. \quad (2)$$

σ_2 satisfies the following conditions [26]:

$$\sigma_2 = \frac{\sigma_1 + \sigma_3}{2}. \quad (3)$$

Combination of equations (1) and (3) gives the expression for the TS-USC under plane strain condition as follows:

$$\sigma_1 = \frac{(2 + b) + 2(1 + b) \sin \varphi}{(2 + b) - 2(1 + b) \sin \varphi} \sigma_3 + \frac{4(1 + b)c \cos \varphi}{(2 + b) - 2(1 + b) \sin \varphi}. \quad (4)$$

2.3. Nonlinear Strain-Softening Behavior. Neither the EPP nor the EB model is utilized to well describe strain-softening behaviors exhibited in average quality rock mass during

tunnelling. Therefore, the softening parameter is introduced to characterize this behavior as follows [40]:

$$\eta = \epsilon_{\theta}^p - \epsilon_r^p, \quad (5)$$

where η is softening parameter, and ϵ_{θ}^p and ϵ_r^p are tangential plastic strain and radial plastic strain, respectively.

When performing the theoretical model derivation, the tangential stress σ_{θ} and radial stress σ_r in the rock mass are assumed to be equal to the σ_1 and σ_3 , respectively. By combining equation (4), the TS-USC under plane strain state that considering the η is given as follows:

$$\sigma_{\theta} = \frac{(2 + b) + 2(1 + b) \sin \varphi(\eta)}{(2 + b) - 2(1 + b) \sin \varphi(\eta)} \sigma_r + \frac{4(1 + b)c(\eta) \cos \varphi(\eta)}{(2 + b) - 2(1 + b) \sin \varphi(\eta)}. \quad (6)$$

Alonso et al. [49] stated that a circular opening can be modeled as a gradual stress reduction from the initial state σ_0 to support force p_i . Figure 2 gives the stress path of a circular opening. η^* is the critical softening parameter of the rock mass, and it is an indicator to determine the transition of the rock mass from the softening state to the residual state [49, 50]. When $\eta = 0$, the rock mass is in the elastic state, which corresponds to the initial ground stress

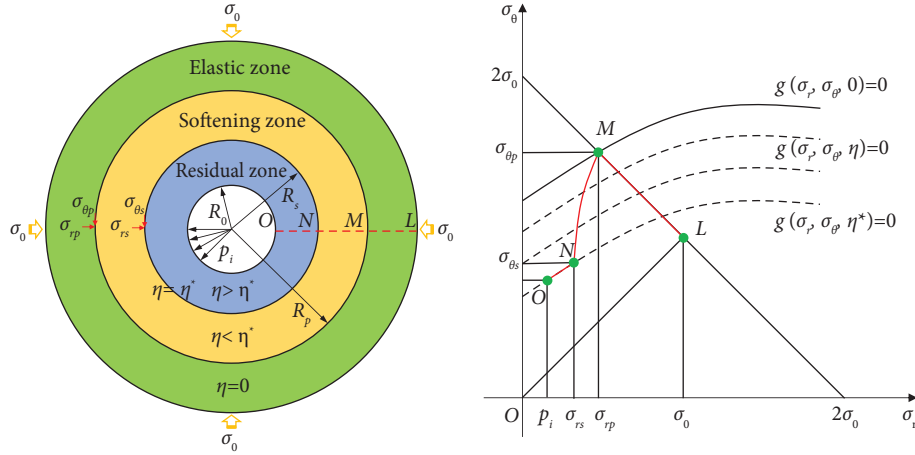


FIGURE 2: Excavation stress path and softening parameter region conversion [49].

state at point L . The radial stress at the elastic-plastic interface (point M) is σ_{rp} , which can be solved by the elastic solution. The rock mass in the zone MN is in softening state, that is, $0 < \eta < \eta^*$. Then, when $\eta \geq \eta^*$ in the zone NO , the rock is in the residual state.

Introducing the softening factor δ , an adopted nonlinear softening model is expressed as follows [51]:

$$\omega(\eta) = \begin{cases} \omega^p + (\omega^p - \omega^r) \left[\delta \left(\frac{\eta}{\eta^*} \right)^2 - (1 + \delta) \left(\frac{\eta}{\eta^*} \right) \right], & 0 < \eta < \eta^*, \\ \omega^r, & \eta \geq \eta^*, \end{cases} \quad (7)$$

where ω^p and ω^r represent the peak and residual values of rock mass strength parameters c and ϕ , respectively. For the δ , it is varying from -1 to 1 . A linear softening model is obtained when $\delta=0$ and a nonlinear softening model for other δ values, while the maximum upward and downward curvatures are obtained when $\delta=1$ and -1 , respectively [51].

Based on the incremental theory of plasticity, the plastic potential function can be expressed as follows [52]:

$$g(\sigma_r, \sigma_\theta, \eta) = \sigma_\theta - K_\psi(\sigma_r, \eta)\sigma_r, \quad (8)$$

where K_ψ is the dilatancy coefficient, and it can be obtained from the following equation [41]:

$$K_\psi = \frac{1 + \sin \psi}{1 - \sin \psi}, \quad (9)$$

where ψ is the dilatancy angle.

2.4. Nonlinear Dilatancy Behavior. The ψ in rocks is not the constant, as it decreases with the increased confining pressure [53]. Alejano and Alonso [50] proposed a model for determining the peak of dilation angle by fitting the experimental data.

$$\psi^p = \frac{\phi^p}{1 + \lg \sigma_c} \lg \frac{\sigma_c}{\sigma_c + 0.1}, \quad (10)$$

where σ_c is the unconfined compression strength.

For a deep circular tunnel, Detournay [54] noted that K_ψ decays exponentially from the peak value K_ψ^p and proposed a fitted expression as follows:

$$K_\psi = 1 + (K_\psi^p - 1)e^{-(\eta/\eta^*)}. \quad (11)$$

By combining equations (9) and (11), ψ is obtained as follows:

$$\psi = \arcsin \left[1 + \left(\frac{1}{\sin \psi^p} - 1 \right) e^{(\eta/\eta^*)} \right]^{-1}. \quad (12)$$

Substituting equations (10) into (12), the nonlinear dilatancy model is obtained as follows:

$$\psi = \arcsin \left\{ 1 + \left[\frac{1}{\sin \left((1 + \lg \sigma_c / \lg(\sigma_3 + 0.1)) \right)} - 1 \right] e^{(\eta/\eta^*)} \right\}^{-1}. \quad (13)$$

3. Numerical Solutions Based on the Finite Difference Method

3.1. Solution for the Elastic Rock Mass. The radial stress σ_r^e , tangential stress σ_θ^e , and radial displacement u_r^e in the elastic zone are expressed as follows [55, 56]:

$$\begin{cases} \sigma_r^e = \sigma_0 + (\sigma_0 - \sigma_{rp}) \left(\frac{R}{r} \right)^2, \\ \sigma_\theta^e = \sigma_0 - (\sigma_0 - \sigma_{rp}) \left(\frac{R}{r} \right)^2, \\ u_r^e = \frac{1 + \mu}{E} (\sigma_0 - \sigma_{rp}) \frac{R^2}{r}, \end{cases} \quad (14)$$

where E is the modulus of elasticity, and μ is Poisson's ratio.

3.2. *Solution for the Plastic Rock Mass.* The equilibrium equation is as follows [42]:

$$\frac{d\sigma_r}{dr} + \frac{\sigma_r - \sigma_\theta}{r} = 0. \quad (15)$$

The radial and circumferential strains of the rock mass under small strain conditions are as follows [41]:

$$\varepsilon_r = \frac{du_r}{dr}, \varepsilon_\theta = \frac{u_r}{r}. \quad (16)$$

The stress at the elastic-plastic interface can be obtained as follows:

$$\sigma_r^e + \sigma_\theta^e = 2\sigma_0. \quad (17)$$

Substituting equations (17) into (6) yields the radial stress at the elastic-plastic interface as follows:

$$\sigma_{rp} = \frac{\sigma_0 [(2+b) - 2(1+b)\sin\varphi^p] - 2(1+b)c^p \cos\varphi^p}{2+b}. \quad (18)$$

The finite difference method is employed to derive stress and strain of the rock mass. Figure 3 gives a schematic diagram of radial stress evolution of the rock mass. The plastic zone is divided into n circles, where $\sigma_{\theta(0)}$ and $\sigma_{r(0)}$ are

tangential and radial stresses at the elastic-plastic interface, and $\sigma_{\theta(n)}$ and $\sigma_{r(n)}$ are the tangential and radial stresses at the excavation surface. The inner and outer boundaries of the i -th ring correspond to the radii $r_{(i-1)}$ and $r_{(i)}$, respectively, and the stress components corresponding to the inner and outer boundaries are $\sigma_{\theta(i-1)}$, $\sigma_{r(i-1)}$ and $\sigma_{\theta(i)}$, $\sigma_{r(i)}$, respectively.

As shown in Figure 3, the stress increment in each ring of plastic zone is as follows:

$$\Delta\sigma_r = \frac{\sigma_{r(n)} - \sigma_{r(0)}}{n}. \quad (19)$$

The radial stress in each ring is calculated by

$$\sigma_{r(i)} = \sigma_{r(i-1)} + \Delta\sigma_r. \quad (20)$$

Substituting equations (20) into (6), the tangential stress of each ring can be given as follows:

$$\begin{aligned} \sigma_{\theta(i)} = & \frac{(2+b) + 2(1+b)\sin\varphi_{(i-1)}}{(2+b) - 2(1+b)\sin\varphi_{(i-1)}} \sigma_{r(i)} \\ & + \frac{4(1+b)c_{(i-1)}\cos\varphi_{(i-1)}}{(2+b) - 2(1+b)\sin\varphi_{(i-1)}}. \end{aligned} \quad (21)$$

Each ring corresponds to different rock strength parameters c and φ can be calculated by the following equation [51]:

$$\omega(\eta_{(i-1)}) = \begin{cases} \omega^p + (\omega^p - \omega^r) \left[\delta \left(\frac{\eta_{(i-1)}}{\eta^*} \right)^2 - (1+\delta) \left(\frac{\eta_{(i-1)}}{\eta^*} \right) \right], & 0 < \eta_{(i-1)} < \eta^*, \\ \omega^r, & \eta_{(i-1)} \geq \eta^*. \end{cases} \quad (22)$$

The equation (15) in finite difference form can be expressed as follows:

$$\frac{\sigma_{r(i)} - \sigma_{r(i-1)}}{r_{(i)} - r_{(i-1)}} + \frac{\sigma_{r(i)} + \sigma_{r(i-1)} - \sigma_{\theta(i)} - \sigma_{\theta(i-1)}}{r_{(i)} + r_{(i-1)}} = 0. \quad (23)$$

Separating $r_{(i-1)}$ and $r_{(i)}$, the ratio of the radii of the inner and outer boundaries in the i -th ring expressed in terms of stress is obtained as follows:

$$\chi_{(i)} = \frac{r_{(i)}}{r_{(i-1)}} = \frac{2\sigma_{r(i-1)} - \sigma_{\theta(i)} - \sigma_{\theta(i-1)}}{2\sigma_{r(i)} - \sigma_{\theta(i)} - \sigma_{\theta(i-1)}}. \quad (24)$$

The elastic strain increment of each ring in the plane strain condition can be derived from the corresponding stress increment of each ring [57].

$$\begin{Bmatrix} \Delta\varepsilon_r^e \\ \Delta\varepsilon_\theta^e \end{Bmatrix} = \frac{1+\mu}{E} \begin{bmatrix} 1-\mu & -\mu \\ -\mu & 1-\mu \end{bmatrix} \begin{Bmatrix} \Delta\sigma_r \\ \Delta\sigma_\theta \end{Bmatrix}, \quad (25)$$

where $\Delta\varepsilon_r^e$ and $\Delta\varepsilon_\theta^e$ are radial and tangential elastic strain increments, respectively.

The incremental η in the i -th ring is expressed as follows:

$$\Delta\eta_{(i)} = \Delta\varepsilon_{\theta(i)}^p - \Delta\varepsilon_{r(i)}^p. \quad (26)$$

It can be obtained from the nonassociated flow rule as follows [57]:

$$\Delta\varepsilon_{r(i)}^p + K_{\psi(i)} \Delta\varepsilon_{\theta(i)}^p = 0, \quad (27)$$

where $\Delta\varepsilon_r^p$ and $\Delta\varepsilon_\theta^p$ are radial and tangential plastic strain increments; and $K_{\psi(i)}$ is the corresponding dilatancy coefficient of the i -th ring.

The total strain in each ring is the total of elastic and plastic strains, then the individual strain components in the i -th ring are expressed as follows:

$$\begin{Bmatrix} \varepsilon_r \\ \varepsilon_\theta \end{Bmatrix} = \begin{Bmatrix} \varepsilon_{r(i-1)} \\ \varepsilon_{\theta(i-1)} \end{Bmatrix} + \begin{Bmatrix} \Delta\varepsilon_r^e \\ \Delta\varepsilon_\theta^e \end{Bmatrix} + \begin{Bmatrix} \Delta\varepsilon_r^p \\ \Delta\varepsilon_\theta^p \end{Bmatrix}. \quad (28)$$

By combining equations (27) and (28), the following relationship between the radial strain $\varepsilon_{r(i)}$ and the tangential strain $\varepsilon_{\theta(i)}$ in the i -th ring is obtained as follows:

$$\varepsilon_{r(i)} + K_{\psi(i)} \varepsilon_{\theta(i)} = \varepsilon_{r(i-1)} + K_{\psi(i)} \varepsilon_{\theta(i-1)} + \Delta\varepsilon_{r(i)}^e + K_{\psi(i)} \Delta\varepsilon_{\theta(i)}^e. \quad (29)$$

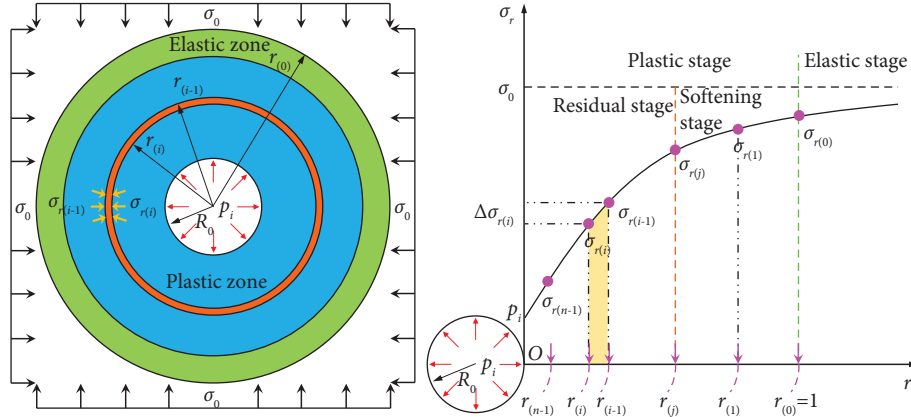


FIGURE 3: Schematic diagram of the finite difference calculation division.

Furthermore, let $\xi_{(i-1)} = \varepsilon_{r(i-1)} + K_{\psi(i)} \varepsilon_{\theta(i-1)} + \Delta \varepsilon_{r(i)}^e + K_{\psi(i)} \Delta \varepsilon_{\theta(i)}^e$ and $\varepsilon_{r(i)}$ and $\varepsilon_{\theta(i)}$ in the i -th ring can be obtained as follows:

$$\begin{cases} \varepsilon_{r(i)} = \xi_{(i-1)} - K_{\psi(i)} \varepsilon_{\theta(i)}, \\ \varepsilon_{\theta(i)} = \frac{(\xi_{(i-1)} - \varepsilon_{r(i)})}{K_{\psi(i)}}. \end{cases} \quad (30)$$

The compatibility equation of deformation is as follows [58]:

$$\frac{d\varepsilon_{\theta}}{dr} + \frac{\varepsilon_{\theta} - \varepsilon_r}{r} = 0. \quad (31)$$

The finite difference form of equation (31) in the i -th ring is as follows:

$$\frac{\varepsilon_{\theta(i)} - \varepsilon_{\theta(i-1)}}{r_{(i)} - r_{(i-1)}} + \frac{\varepsilon_{\theta(i)} + \varepsilon_{\theta(i-1)} - \varepsilon_{r(i)} - \varepsilon_{r(i-1)}}{r_{(i)} + r_{(i-1)}} = 0. \quad (32)$$

The ratio of the inner and outer boundary radii of the i -th ring expressed in terms of strain is as follows:

$$\chi_{(i)} = \frac{r_{(i)}}{r_{(i-1)}} = \frac{2\varepsilon_{\theta(i-1)} - \varepsilon_{r(i)} - \varepsilon_{r(i-1)}}{2\varepsilon_{\theta(i)} - \varepsilon_{r(i)} - \varepsilon_{r(i-1)}}. \quad (33)$$

Substituting equations (30) into (33) yields

$$\begin{cases} \varepsilon_{r(i)} = \frac{2\chi_{(i)}\xi_{(i-1)}/K_{\psi(i)} - (\chi_{(i)} - 1)\varepsilon_{r(i-1)} - 2\varepsilon_{\theta(i-1)}}{2\chi_{(i)}/K_{\psi(i)} + \chi_{(i)} - 1}, \\ \varepsilon_{\theta(i)} = \frac{2\varepsilon_{\theta(i-1)} + (\chi_{(i)} - 1)(\varepsilon_{r(i-1)} + \xi_{(i-1)})}{\chi_{(i)}(2 + K_{\psi(i)}) - K_{\psi(i)}}. \end{cases} \quad (34)$$

The plastic strain increment for the i -th ring is as follows:

$$\begin{cases} \Delta \varepsilon_{r(i)}^p = \varepsilon_{r(i)} - \varepsilon_{r(i-1)} - \Delta \varepsilon_{r(i)}^e, \\ \Delta \varepsilon_{\theta(i)}^p = \varepsilon_{\theta(i)} - \varepsilon_{\theta(i-1)} - \Delta \varepsilon_{\theta(i)}^e. \end{cases} \quad (35)$$

Combining equations (25), (34), and (35), the expression for η of the i -th ring is obtained as follows:

$$\eta_{(i)} = \eta_{(i-1)} + \Delta \eta_{(i)} = \eta_{(i-1)} + (\Delta \varepsilon_{\theta(i)}^p - \Delta \varepsilon_{r(i)}^p). \quad (36)$$

3.3. *Plastic Radius.* The boundary conditions in the solution are as follows:

$$\sigma_r|_{r=R_0} = p_i, \sigma_r|_{r=R_s} = \sigma_{rs}. \quad (37)$$

Combining equation (14) yields the residual radius as follows:

$$R_s = R_0 \times \left(\frac{c^r \cot \varphi^r + \sigma_{rs}}{c^r \cot \varphi^r + p_i} \right)^{\frac{(2+b)-2(1+b) \sin \varphi^r/4(1+b) \sin \varphi^r}{1}}. \quad (38)$$

Superimposing n equation (33) yields

$$\frac{R_0}{R_p} = \frac{r_{(n)}}{r_{(0)}} = \prod_{i=1}^n \chi_{(i)}. \quad (39)$$

The radius of plastic zone is as follows:

$$R_p = \frac{R_0}{\prod_{i=1}^n \chi_{(i)}}. \quad (40)$$

Furthermore, the radius of the i -th ring is as follows:

$$r_{(i)} = R_p \times \prod_{i=0}^i \chi_{(i)}. \quad (41)$$

3.4. *Displacement in the Plastic Zone.* Substituting equations (35) and (41) into (16), the radial displacement of the i -th ring can be obtained as follows:

$$u_{r(i)} = \varepsilon_{\theta(i)} r_{(i)} = R_p \frac{2\varepsilon_{\theta(i-1)} + (\chi_{(i)} - 1)(\varepsilon_{r(i-1)} + \xi_{(i-1)})}{\chi_{(i)}(2 + K_{\psi(i)}) - K_{\psi(i)}} \prod_{i=1}^i \chi_{(i)}. \quad (42)$$

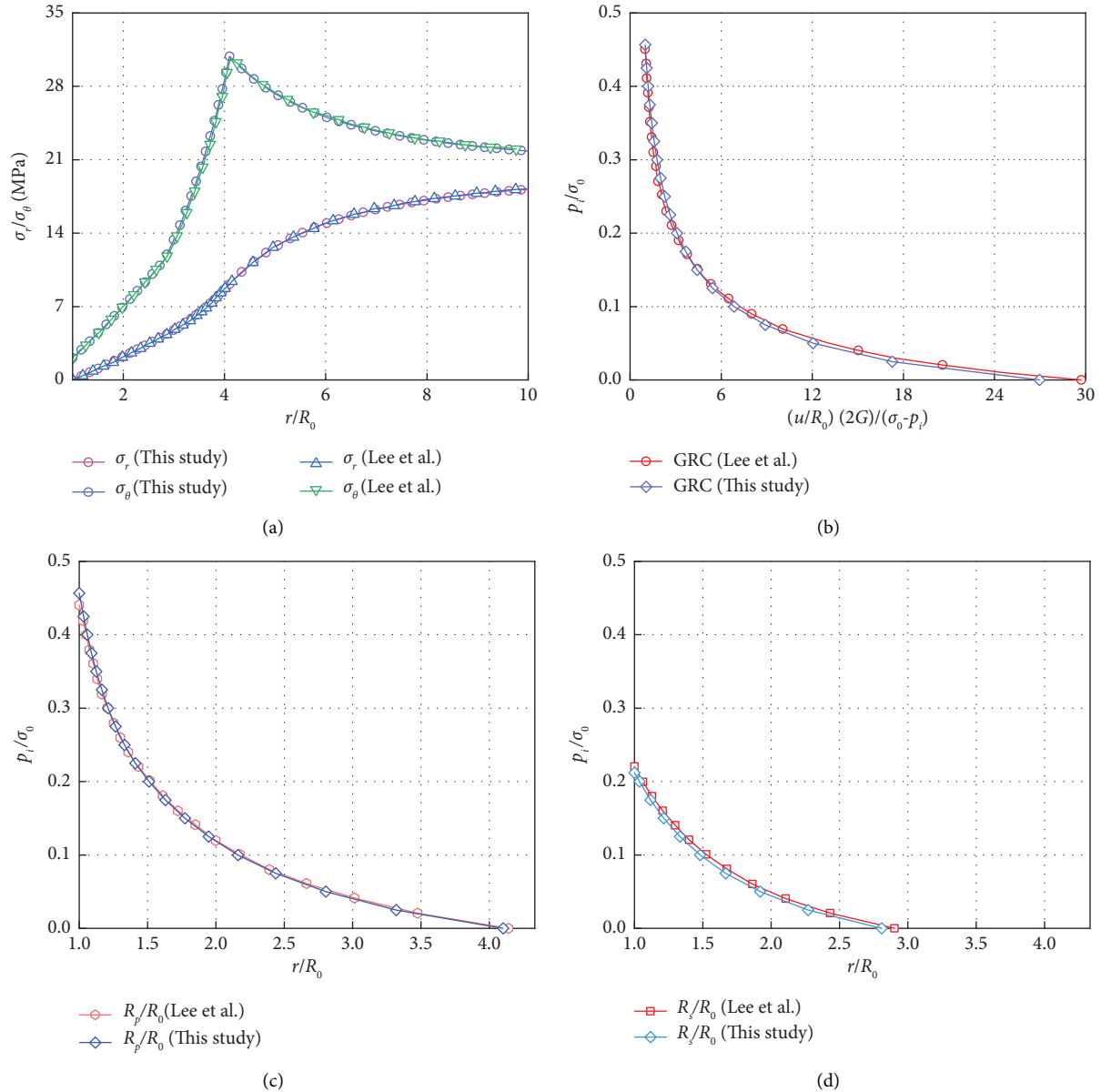


FIGURE 4: A result comparison between the proposed solution and referenced example. (a) Rock stress. (b) Rock displacement. (c) Relationship between R_p and p_i . (d) Relationship between R_s and p_i [41].

4. Verification Examples and Comparison

The results in the literature [41, 49] are referred to verify the soundness of the solution proposed in this paper. The parameters used for validation are as follows: σ_0 , R_0 , E , and μ are 20 MPa, 3 m, 10 GPa and 0.25, respectively. φ^p and φ^r are 30° and 22° , while c^p and c^r are 1.0 MPa and 0.7 MPa, respectively. η^* is fixed as 0.008. It is worth noting that the TS-USC of the proposed solution is converted to the M-C yield criterion (by setting b to 0), for consistency with that in the literature [41]. A comparison of the results obtained from the two solutions is displayed in Figure 4, which verified the validity of the solution proposed in this study.

Also, other interesting attempts are performed to solve the tunnel unloading problem and investigate the influence

of the postpeak drop modulus on elastoplastic behaviors of the rock mass [59–61]. Here, the results reported in [60, 61] were chosen as representative cases for comparison. According to Alejano et al. [60], three strain-softening models with considering the constant/variable drop modulus (M) and the constant/variable dilatancy (ψ) were proposed for the purpose of characterizing the postfailure behaviors of the poor, average, and good quality rock masses. The results in terms of p_i and rock displacement u_0 , with a reference to the average quality rock mass type, are depicted in Figure 5(a). As can be observed in the figure, for the average quality rock masses, the GRC acquired by the model proposed in this study is approximately close to the referred strain-softening model with a constant drop modulus and a constant dilatancy. However, u_0 values

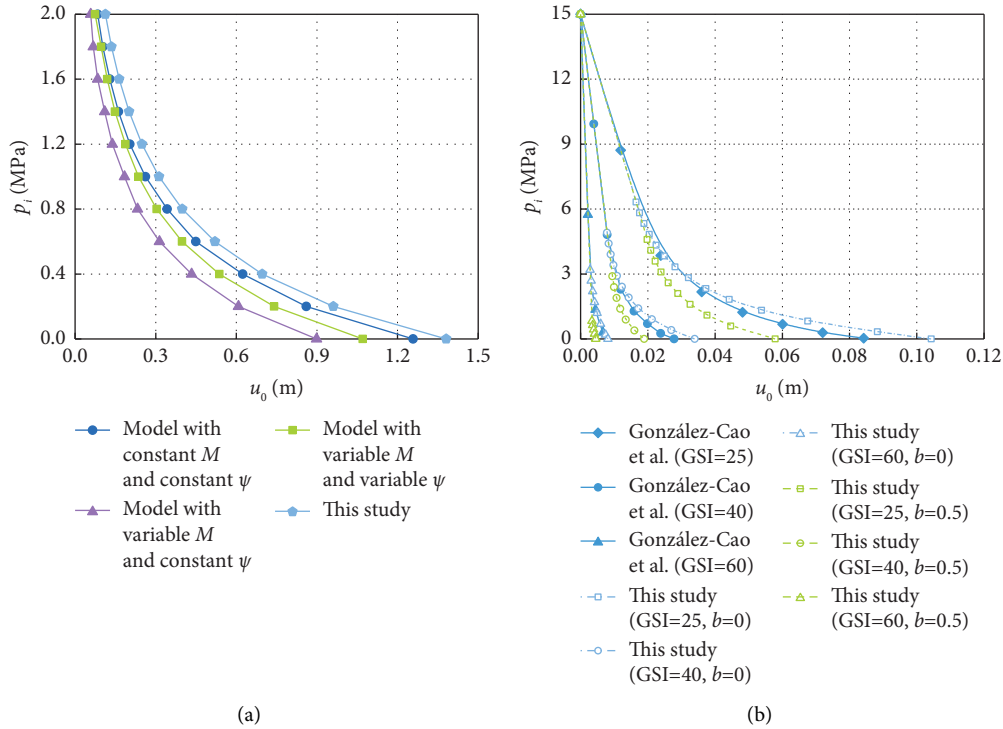


FIGURE 5: Comparisons between the models considering the drop modulus and unloading issue. (a) The model considering the drop modulus. (b) The model considering the unloading problem [60, 61].

gained by the proposed model are all larger than those determined by the abovementioned three models. It delivers a clear fact that the deliberate characterization of the postfailure behaviors is essential for tunnel stability analysis.

For comparison purposes, the computed rock displacements for the unloaded case by the González-Cao et al. [61] together with results obtained with the proposed model under two different b values are represented in Figure 5(b). It can be seen that u_0 values under the same p_i levels determined by the proposed model is also slightly larger than those calculated by the referred model. Obviously, the intermediate principal stress effect contributes to the self-stabilization of the rock mass. This can be confirmed by the decrease of u_0 values when b increases from 0 to 1. The rock displacement differences between the models decrease with the increased GSI values (which means the improvement of the rock mass quality). It is notable that, for different quality rock masses, some errors might arise if stability analysis is not based on the suitable models, particularly for the poor to average quality rock masses. Therefore, to obtain a reliable rock mass response, it is crucial to develop reliable models to describe rock behaviors.

5. Parametric Analysis on Dilatancy Behavior of the Rock Mass in the Plastic Zone

Parametric analysis on dilatancy behaviors of the rock mass in the plastic zone is conducted in this section. The relevant parameters utilized for investigation are referred from the literature [60]. The details are listed in Table 1.

5.1. Influence of b . When b is the variable, ψ under different p_i , η^* , and δ show similar curve characteristics; so, a representative scenery of $p_i=0$, $\eta^*=0.006$, and $\delta=0.5$ are selected to analyze the variation feature of ψ in the rock mass, as shown in Figure 6. The red circle in the figure is the demarcation point of the softening zone and the residual zone of the rock mass. It can be observed that, for different b , ψ tends to decrease from deep rock mass to the excavation surface, and the maximum ψ value is found at the elastic-plastic interface. ψ in the softening zone is significantly larger than that in the residual zone, indicating that dilatancy effect in the softening zone is more notable than that in the residual zone. The reduction rate of ψ in the softening zone is also considerably higher than that in the residual zone. It is evident that intermediate principal stress only diminishes the plastic radius but also determines the progression pattern of ψ with depth variations of the rock mass. The magnitude of ψ at the elastic-plastic interface is dependent on b . When $b=0$, ψ at elastic-plastic interface is 5.85° ; ψ at the interface increases with the increased b ; and ψ acquires the maximum value of 7.47° when $b=1$. As the intermediate principal stress effect increases (i.e., the increasing b values), the peak values of ψ increases; also, the dilatancy effect of the rock mass is more significant when the intermediate principal stress is considered than when it is not considered.

5.2. Influence of η^* . The thresholds of η^* is generally in range of 0.001–0.01 [62]. Therefore, η^* are set as 0.001, 0.002, 0.004, 0.006, 0.008, and 0.01, respectively, in the analysis. The results of ψ with varying η^* for the selected scenery of $p_i=0$,

TABLE 1: Parameters used for analysis.

R_0 (m)	σ_0 (MPa)	E (MPa)	μ	σ_c (MPa)	c^p (MPa)	c^r (MPa)	ϕ^p (°)	ϕ^r (°)
7	12	3837	0.25	23	0.744	0.397	24.81	15.67

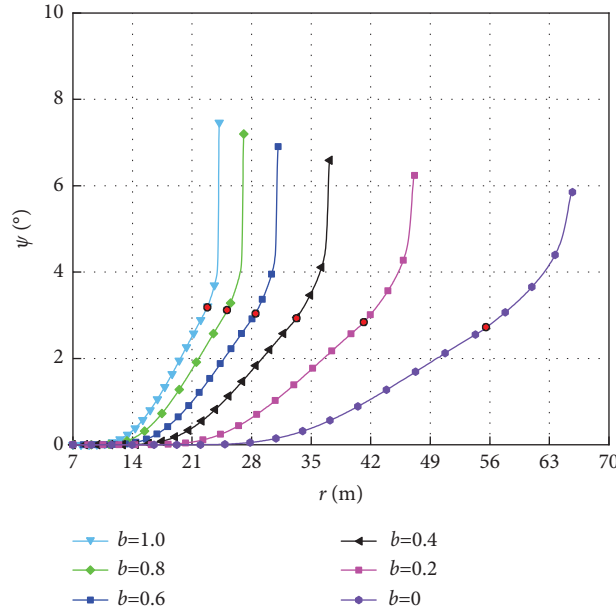


FIGURE 6: Influence of different b on ψ of the rock mass in the plastic zone.

$b = 0.4$, and $\delta = 0.5$ are shown in Figure 7. It confirms that ψ at the elastic-plastic interface is constant (all values are 6.59°) for different η^* , indicating that the magnitude of ψ is not influenced by η^* . Similarly, ψ decreases gradually from deep rock mass to the excavation surface, but the decay rate varies significantly under different η^* . The decay rate of ψ increases sharply with the decrease of η^* . The smaller the η^* , the less the range of the softening zone, which causing the residual zone to occupy a larger proportion. For the rock mass with the η^* value of 0.001, it clearly observes a drop-down decrease in ψ from the peak, reflecting brittle failure caused by large plastic of the rock mass at the elastic-plastic interface.

5.3. Influence of δ . δ controls postpeak softening behavior of the rock mass, and δ values of -1 , -0.5 , 0 , 0.5 , and 1 are selected to analyze evolutionary characteristics of ψ with different softening behaviors. The results of ψ for $p_i = 0$, $\eta^* = 0.006$, and $b = 0.4$ are displayed in Figure 8. δ of the rock mass shows an effect on the size of the plastic radius, which gradually increases from 35 m to 37.8 m as the δ goes from -1 to 1 . The fixed value of 6.59° for ψ at the elastic-plastic interface indicates that δ does not influence the magnitude of ψ . For different δ , the variation pattern of ψ in the residual zone is basically the same in the radial direction, and they all exhibit a two-stage approximately linear decrease. In the softening zone, the variability of ψ is significant. The rate of reduction of ψ , compared to the linear softening ($\delta = 0$), is

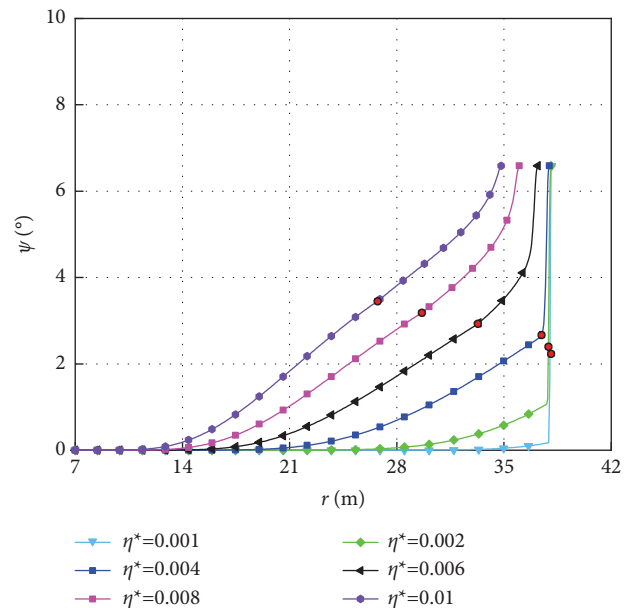


FIGURE 7: Influence of different η^* on the ψ of the rock mass in the plastic zone.

more drastic for depressed nonlinear strain-softening behavior ($\delta = 0.5$ and 1). ψ in the softening zone under convex nonlinear strain-softening behavior falls off rapidly as it approaches the residual zone.

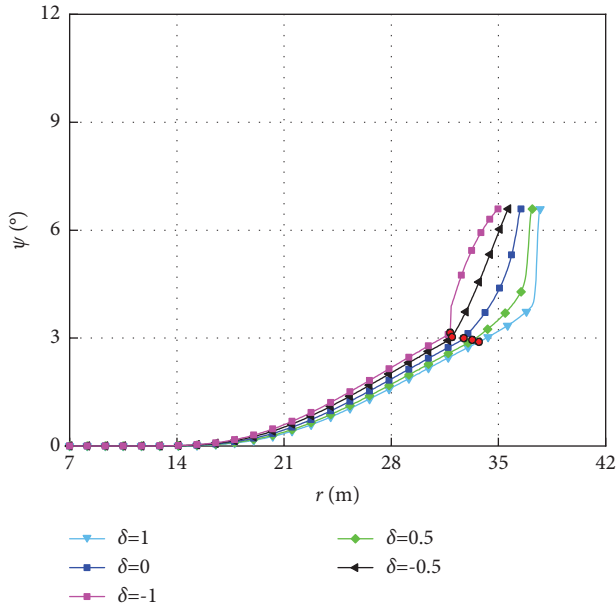


FIGURE 8: Influence of different δ on the ψ of the rock mass in the plastic zone.

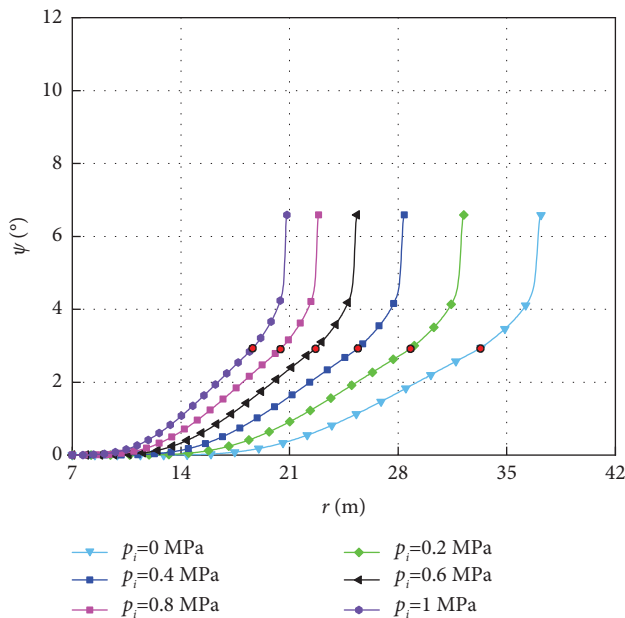


FIGURE 9: Influence of different p_i on the ψ of the rock mass in the plastic zone.

5.4. Influence of p_i . The influence of varying p_i on ψ , for the scenery of $\eta^* = 0.006$, $b = 0.4$, and $\delta = 0.5$, are displayed in Figure 9. ψ tends to decrease from deep rock mass to the excavation surface, while ψ at the elastic-plastic interface is constant, i.e., 6.59° . ψ at residual-softening interfaces under different p_i are also the same, indicating that support force does not control the magnitude of the ψ values in plastic zone of rock mass for the given η^* , b , and δ values.

6. Conclusion

- (1) The TS-USC is introduced to establish an axisymmetric elastoplastic finite difference solution of a deep circular opening, which considers the intermediate principal stress, nonlinear dilatancy, and nonlinear strain-softening behaviors of the rock mass. The solution introduces b and δ to characterize the action degree of intermediate principal stress and strain-softening behavior of the rock mass. The variations of the introduced parameters can conveniently reflect the variability of derivation results controlled by different yield criteria, dilatancy, and strain-softening behaviors, which are of wider theoretical and practical application.
- (2) Parametric analysis revealed that the maximum value of ψ under different b occurs at the elastic-plastic interface. The values and reduction rates of ψ in the softening zone are significantly larger than those in the residual zone. The peak value of ψ increases with the increased b , indicating that intermediate principal stress mainly affects the peak value of ψ , and the dilatancy effect of rock mass is more pronounced when considering the intermediate principal stress than when it is not.
- (3) The magnitude of ψ at the elastic-plastic interface is not affected by η^* , but the decay rate of ψ due to the change of η^* varies significantly. The decay rate of ψ dramatically increases as η^* decreases. The smaller the η^* , the smaller the softening zone and the more the residual zone. The rock strength decreases rapidly, resulting in a drop-type reduction of the ψ from the peak when $\eta^* = 0.001$, while causing brittle failure with large plastic deformation.
- (4) The softening behavior of the rock mass affects the magnitude of the plastic radius but does not affect values of ψ at the elastic-plastic interface. The variation pattern of ψ in the residual zone is similar for different δ , but the difference in variation of ψ in the softening zone is obvious.
- (5) For a given intermediate principal stress state, critical softening parameter and softening behavior of the rock mass (reflecting by parameters of b , η^* , and δ), the value and development form of the ψ in the plastic zone is independent of the support force.

Data Availability

The data used to support the findings of this study are included within the article.

Conflicts of Interest

The authors declare that there are no conflicts of interest.

Acknowledgments

This research was financially supported by the National Natural Science Foundation of China (grant no. 52208386) and the Scientific Research and Innovation Project of the China Railway First Survey and Design Institute Group Co., Ltd. (grant no. 2022KY17ZD(ZNJC)-01).

References

- [1] A. Hedayat and J. Weems, "The elasto-plastic response of deep tunnels with damaged zone and gravity effects," *Rock Mechanics and Rock Engineering*, vol. 52, no. 12, pp. 5123–5135, 2019.
- [2] M. R. Zareifard, "Ground reaction curve for deep circular tunnels in strain-softening Mohr–Coulomb rock masses considering the damaged zone," *International Journal of Geomechanics*, vol. 20, no. 10, Article ID 04020190, 2020.
- [3] K. Wu, Z. S. Shao, M. Sharifzadeh, Z. F. Chu, and S. Qin, "Analytical approach to estimating the influence of shotcrete hardening property on tunnel response," *Journal of Engineering Mechanics*, vol. 148, no. 1, Article ID 04021127, 2022.
- [4] A. Ghorbani and H. Hasanzadehshooili, "A comprehensive solution for the calculation of ground reaction curve in the crown and sidewalls of circular tunnels in the elastic-plastic-EDZ rock mass considering strain softening," *Tunnelling and Underground Space Technology*, vol. 84, pp. 413–431, 2019.
- [5] J. L. Qiu, F. F. Fan, C. P. Zhang, J. X. Lai, K. Wang, and F. Y. Niu, "Response mechanism of metro tunnel structure under local collapse in loess strata," *Environmental Earth Sciences*, vol. 81, 2022.
- [6] A. Showkati, H. Salari-rad, and M. Hazrati Aghchai, "Predicting long-term stability of tunnels considering rock mass weathering and deterioration of primary support," *Tunnelling and Underground Space Technology*, vol. 107, Article ID 103670, 2021.
- [7] Q. Zhang, H. Y. Wang, Y. J. Jiang, M. M. Lu, and B. S. Jiang, "A numerical large strain solution for circular tunnels excavated in strain-softening rock masses," *Computers and Geotechnics*, vol. 114, Article ID 103142, 2019.
- [8] J. F. Zou, C. Li, and F. Wang, "A new procedure for ground response curve (GRC) in strain-softening surrounding rock," *Computers and Geotechnics*, vol. 89, pp. 81–91, 2017.
- [9] E. Kabwe, M. Karakus, and E. K. Chanda, "Time-dependent solution for non-circular tunnels considering the elasto-viscoplastic rock mass," *International Journal of Rock Mechanics and Mining Sciences*, vol. 133, Article ID 104395, 2020.
- [10] E. Hoek and E. T. Brown, "Practical estimates of rock mass strength," *International Journal of Rock Mechanics and Mining Sciences*, vol. 34, no. 8, pp. 1165–1186, 1997.
- [11] A. Z. Lu, G. S. Xu, F. Sun, and W. Q. Sun, "Elasto-plastic analysis of a circular tunnel including the effect of the axial in situ stress," *International Journal of Rock Mechanics and Mining Sciences*, vol. 47, no. 1, pp. 50–59, 2009.
- [12] R. R. Osgoui and P. Oreste, "Elasto-plastic analytical model for the design of grouted bolts in a Hoek-Brown medium," *International Journal for Numerical and Analytical Methods in Geomechanics*, vol. 34, no. 16, pp. 1651–1686, 2018.
- [13] B. C. Haimson, "The hydrofracturing stress measuring method and recent field results," *International Journal of Rock Mechanics and Mining Sciences & Geomechanics Abstracts*, vol. 15, no. 4, pp. 167–178, 1978.
- [14] S. S. Xu, E. L. Ma, J. X. Lai et al., "Diseases failures characteristics and countermeasures of expressway tunnel of water-rich strata: d characteristics and countermeasures of expressway tunnel of water-rich strata: a case study case study," *Engineering Failure Analysis*, vol. 134, Article ID 106056, 2022.
- [15] H. Kang, X. Zhang, L. Si, Y. Wu, F. Gao, and F. Gao, "In-situ stress measurements and stress distribution characteristics in underground coal mines in China," *Engineering Geology*, vol. 116, no. 3-4, pp. 333–345, 2010.
- [16] E. L. Ma, J. X. Lai, S. S. Xu, X. H. Shi, J. Zhang, and Y. J. Zhong, "Failure analysis and treatments of a loess tunnel being constructed in ground fissure area," *Engineering Failure Analysis*, vol. 134, Article ID 106034, 2022.
- [17] E. Kabwe, M. Karakus, and E. K. Chanda, "Proposed solution for the ground reaction of non-circular tunnels in an elastic-perfectly plastic rock mass," *Computers and Geotechnics*, vol. 119, Article ID 103354, 2020.
- [18] K. Mogi, "Effect of the intermediate principal stress on rock failure," *Journal of Geophysical Research*, vol. 72, no. 20, pp. 5117–5131, 1967.
- [19] Z. Z. Liang, B. Gong, and W. R. Li, "Instability analysis of a deep tunnel under triaxial loads using a three-dimensional numerical method with strength reduction method," *Tunnelling and Underground Space Technology*, vol. 86, pp. 51–62, 2019.
- [20] J. F. Zou, L. Liu, and M. Y. Xia, "Simple approach for solution of the quasi-plane-strain problem in a circular tunnel in a strain-softening rock mass considering the out-of-plane stress effect," *Underground Space*, vol. 5, no. 4, pp. 339–353, 2020.
- [21] E. Kabwe, "Confining stress effect on the elastoplastic ground reaction considering the Lode angle dependence," *International Journal of Mining Science and Technology*, vol. 30, no. 3, pp. 431–440, 2020.
- [22] B. Single, R. K. Goel, V. K. Mehrotra, S. K. Garg, and M. R. Allu, "Effect of intermediate principal stress on strength of anisotropic rock mass," *Tunnelling and Underground Space Technology*, vol. 13, no. 1, pp. 71–79, 1998.
- [23] W. Q. Cai, H. H. Zhu, W. H. Liang et al., "Three-dimensional forward analysis and real-time design of deep tunneling based on digital in-situ testing," *International Journal of Mechanical Sciences*, vol. 226, Article ID 107385, 2022.
- [24] M. H. Yu, *Unified Strength Theory and its Applications*, Springer and Verlag, Berlin Heidelberg, Germany, 2004.
- [25] M. H. Yu, "Advances in strength theories for materials under complex stress state in the 20th Century," *Applied Mechanics Reviews*, vol. 55, no. 3, pp. 169–218, 2002.
- [26] S. Q. Xu and M. H. Yu, "The effect of the intermediate principal stress on the ground response of circular openings in rock mass," *Rock Mechanics and Rock Engineering*, vol. 39, no. 2, pp. 169–181, 2006.
- [27] C. G. Zhang, J. H. Zhao, Q. H. Zhang, and X. D. Hu, "A new closed-form solution for circular openings modeled by the Unified Strength Theory and radius-dependent Young's modulus," *Computers and Geotechnics*, vol. 42, pp. 118–128, 2012.
- [28] X. F. Li, S. J. Du, and B. Chen, "Unified analytical solution for deep circular tunnel with consideration of seepage pressure, grouting and lining," *Journal of Central South University*, vol. 24, pp. 1483–1493, 2017.
- [29] Z. Y. Sun, D. L. Zhang, Q. Fang, G. S. Dui, and Z. F. Chu, "Analytical solutions for deep tunnels in strain-softening rocks modeled by different elastic strain definitions with

- the unified strength theory,” *Science China Technological Sciences*, vol. 65, no. 10, pp. 2503–2519, 2022.
- [30] X. R. Hu and M. H. Yu, “New research on failure criterion for geomaterial,” *Chinese Journal of Rock Mechanics and Engineering*, vol. 23, no. 18, pp. 3037–3043, 2004.
- [31] X. Y. Cao, J. H. Zhao, J. Q. Ji, J. L. Sun, and M. M. Qiu, “Triple-shear unified solution for bearing capacity of unsaturated soft soil foundations with hard crust,” *Geofluids*, vol. 2022, Article ID 4758311, pp. 1–10, 2022.
- [32] Q. Zhu, J. H. Zhao, C. G. Zhang, Y. Li, and S. Wang, “Elastic–brittle–plastic analysis of double-layered combined thick-walled cylinder under internal pressure,” *Journal of Pressure Vessel Technology*, vol. 138, no. 1, Article ID 011201, 2016.
- [33] Y. W. Qin, J. L. Qiu, J. X. Lai et al., “Seepage characteristics in loess strata subjected to single point water supply,” *Journal of Hydrology*, vol. 609, Article ID 127611, 2022.
- [34] Z. Y. Sun, D. L. Zhang, Q. Fang, D. P. Liu, and G. S. Dui, “Displacement process analysis of deep tunnels with grouted rockbolts considering bolt installation time and bolt length,” *Computers and Geotechnics*, vol. 140, Article ID 104437, 2021.
- [35] Y. Cao, L. Chen, J. H. Xu, C. Li, and W. Zhang, “Unified analytical solutions of circular tunnel excavated in an elastic-brittle-plastic rock mass considering blast-induced damage and dead weight loading,” *Advances in Civil Engineering*, vol. 2021, Article ID 5537963, pp. 1–12, 2021.
- [36] K. Guan, W. C. Zhu, X. G. Liu, and J. Wei, “Finite strain analysis of squeezing response in an elastic-brittle-plastic weak rocks considering the influence of axial stress,” *Tunnelling and Underground Space Technology*, vol. 97, Article ID 103254, 2020.
- [37] F. Song and A. Rodriguez-Dono, “Numerical solutions for tunnels excavated in strain-softening rock masses considering a combined support system,” *Applied Mathematical Modelling*, vol. 92, pp. 905–930, 2021.
- [38] X. Z. Wu, Y. J. Jiang, and Z. C. Guan, “A modified strain-softening model with multi-post-peak behaviours and its application in circular tunnel,” *Engineering Geology*, vol. 240, pp. 21–33, 2018.
- [39] M. C. Weng, L. S. Tsai, C. Y. Liao, and F. S. Jeng, “Numerical modeling of tunnel excavation in weak sandstone using a time-dependent anisotropic degradation model,” *Tunnelling and Underground Space Technology*, vol. 25, no. 4, pp. 397–406, 2010.
- [40] P. A. Vermeer and R. D. Borst, “Non-associated plasticity for soils, concrete and rock,” *Heron*, vol. 29, no. 3, pp. 1–64, 1984.
- [41] Y. K. Lee and S. Pietruszczak, “A new numerical procedure for elasto-plastic analysis of a circular opening excavated in a strain-softening rock mass,” *Tunnelling and Underground Space Technology*, vol. 23, no. 5, pp. 588–599, 2008.
- [42] K. H. Park, B. Tontavanich, and J. G. Lee, “A simple procedure for ground response curve of circular tunnel in elastic-strain softening rock masses,” *Tunnelling and Underground Space Technology*, vol. 23, no. 2, pp. 151–159, 2008.
- [43] L. Cui, J. J. Zheng, R. J. Zhang, and Y. K. Dong, “Elasto-plastic analysis of a circular opening in rock mass with confining stress-dependent strain-softening behaviour,” *Tunnelling and Underground Space Technology*, vol. 50, pp. 94–108, 2015.
- [44] K. H. Park, “Similarity solution for a spherical or circular opening in elastic-strain softening rock mass,” *International Journal of Rock Mechanics and Mining Sciences*, vol. 71, pp. 151–159, 2014.
- [45] Q. Zhang, B. S. Jiang, S. L. Wang, X. R. Ge, and H. Q. Zhang, “Elasto-plastic analysis of a circular opening in strain-softening rock mass,” *International Journal of Rock Mechanics and Mining Sciences*, vol. 50, pp. 38–46, 2012.
- [46] X. G. Zhao and M. Cai, “Influence of plastic shear strain and confinement-dependent rock dilation on rock failure and displacement near an excavation boundary,” *International Journal of Rock Mechanics and Mining Sciences*, vol. 47, no. 5, pp. 723–738, 2010.
- [47] X. G. Zhao, M. F. Cai, and M. Cai, “Considerations of rock dilation on modeling failure and deformation of hard rocks—a case study of the mine-by test tunnel in Canada,” *Journal of Rock Mechanics and Geotechnical Engineering*, vol. 2, no. 4, pp. 338–349, 2010.
- [48] K. Yi, H. P. Kang, W. J. Ju, Y. D. Liu, and Z. G. Lu, “Synergistic effect of strain softening and dilatancy in deep tunnel analysis,” *Tunnelling and Underground Space Technology*, vol. 97, Article ID 103280, 2020.
- [49] E. Alonso, L. R. Alejano, F. Varas, G. Fdez-Manin, and C. Carranza-Torres, “Ground response curves for rock masses exhibiting strain-softening behaviour,” *International Journal for Numerical and Analytical Methods in Geomechanics*, vol. 27, no. 13, pp. 1153–1185, 2003.
- [50] L. R. Alejano and E. Alonso, “Considerations of the dilatancy angle in rocks and rock masses,” *International Journal of Rock Mechanics and Mining Sciences*, vol. 42, no. 4, pp. 481–507, 2005.
- [51] M. R. Zareifard, “A new semi-numerical method for elasto-plastic analysis of a circular tunnel excavated in a Hoek-Brown strain-softening rock mass considering the blast-induced damaged zone,” *Computers and Geotechnics*, vol. 122, Article ID 103476, 2020.
- [52] R. Hill, *The Mathematical Theory of Plasticity*, Oxford University Press, New York City, NY, USA, 1950.
- [53] P. Bésuelle, J. Desrues, and S. Raynaud, “Experimental characterisation of the localisation phenomenon inside a Vosges sandstone in a triaxial cell,” *International Journal of Rock Mechanics and Mining Sciences*, vol. 37, no. 8, pp. 1223–1237, 2000.
- [54] E. Detournay, “Elastoplastic model of a deep tunnel for a rock with variable dilatancy,” *Rock Mechanics and Rock Engineering*, vol. 19, no. 2, pp. 99–108, 1986.
- [55] S. K. Sharan, “Elastic-brittle-plastic analysis of circular openings in Hoek-Brown media,” *International Journal of Rock Mechanics and Mining Sciences*, vol. 40, no. 6, pp. 817–824, 2003.
- [56] S. K. Sharan, “Analytical solutions for stresses and displacements around a circular opening in a generalized Hoek-Brown rock,” *International Journal of Rock Mechanics and Mining Sciences*, vol. 45, no. 1, pp. 78–85, 2008.
- [57] E. T. Brown, J. W. Bray, B. Ladanyi, and E. Hoek, “Ground response curves for rock tunnels,” *Journal of Geotechnical Engineering*, vol. 109, no. 1, pp. 15–39, 1983.
- [58] A. L. Florence and L. E. Schwer, “Axisymmetric compression of a Mohr-Coulomb medium around a circular hole,” *International Journal for Numerical and Analytical Methods in Geomechanics*, vol. 2, no. 4, pp. 367–379, 1978.
- [59] L. R. Alejano, E. Alonso, A. Rodriguez-Dono, and G. Fernandez-Manin, “Application of the convergence-confinement method to tunnels in rock masses exhibiting Hoek-Brown strain-softening behaviour,” *International Journal of Rock Mechanics and Mining Sciences*, vol. 47, no. 1, pp. 150–160, 2010.
- [60] L. R. Alejano, A. Rodriguez-Dono, E. Alonso, and G. Fdez-Manin, “Ground reaction curves for tunnels excavated in different quality rock masses showing several types of post-

failure behaviour,” *Tunnelling and Underground Space Technology*, vol. 24, no. 6, pp. 689–705, 2009.

- [61] J. González-Cao, F. Varas, F. G. Bastante, and L. R. Alejano, “Ground reaction curves for circular excavations in non-homogeneous, axisymmetric strain-softening rock masses,” *Journal of Rock Mechanics and Geotechnical Engineering*, vol. 5, no. 6, pp. 431–442, 2013.
- [62] L. Alejano, E. Alonso, G. Fernández-Manin, and F. G. Bastante, “Influence of post-peak properties in the application of the convergence-confinement method for designing underground excavations,” in *Proceedings of the 5th International Conference and Exhibition on Mass Mining*, pp. 793–802, Luleå, Sweden, June 2008.